International Journal of Engineering

Journal Homepage: www.ije.ir

RESEARCH NOTE

A New Optimization of Segmented Interior Permanent Magnet Synchronous Motor Based on Increasing Flux Weakening Range and Output Torque

M. Arehpanahi*, E. Kheiry

Electrical engineering department, Tafresh University, Tafresh, Iran

PAPER INFO

Paper history:
Received 07 August 2019
Received in revised form 01 January 2019
Accepted 04 March 2020

Keywords:
Flux Weakening Range
Interior Permanent Magnet
Optimization
Segmented Permanent Magnet

ABSTRACT

In this paper a new optimization function for increasing the flux weakening range and output torque value of segmented interior permanent magnet synchronous motor (SIPMSM) is presented. In proposed objective function normalized characteristic current and saliency ratio are considered as two optimization variables during optimization process. The focus of this paper is rotor structure design such as PM segmentation technique and new flux barrier design. Increasing the constant power speed range (CPSR) of SIPMSM is done by minimization of characteristic current. This minimization leads to decreasing the output torque therefore in this paper using maximization of saliency ratio, this problem during optimization process will overcomed. For calculation resource reduction a detailed design of PM segmented and flux barriers configuration in rotor structure is carried out by simplified magnetic equivalent circuit of SIPMSM. The output results of proposed magnetic equivalent circuit which is contained PM flux linkage and dq inductances, are verified by Finite Element Method. Simulation results demonstrate that the CPSR of optimized SIPMSM has been doubled and its output torque has been increased related to the typical design.

***doi**: 10.5829/ije.2020.33.06c.09*

NOMENCLATURE

V_s	Stator voltage (v)	ρ	Saleincy ratio
CPSR	Constant Power Speed Range	$\Re_s$	Stator reluctnace reluctnace(H/m)
D, L	stator bore , machine axial length, (m)	$\Re_r$	rotor reluctnace(H/m)
p	pole pairs	$2\Re_g$	Half of the Air gap reluctance(H/m)
k_c	carter coefficient	$\Re_{mm}$	iron bridges above the flux barrier reluctnace(H/m)
$K_{w1}, N_{ph},$	winding coefficient, number of phase turns,	$\Re_{ml}$	leakage flux reluctnace(H/m)
k_{1ad}, k_{ad}, k_1	They are expressed in Appendix	$\Re_{ib}$	Iron bridges between PMs, reluctnace(H/m)
Greek Symbols		$2\Re_{mosi}$	PM segmented reluctnace (H/m)
γ	Number of PM segmented	λ	Flux linkage (Wb)

1. INTRODUCTION

Operation of electric machines which are employed as electric vehicles in over wide speed range is necessary [1–3]. Nominal power preservation of electric machines at speeds higher than nominal value requires flux weakening capability. Flux weakening capability is defined as maximum accessible speed value divided by nominal speed which is called Constant Power Speed Range (CPSR). For example the CPSR of a conventional efficient line-start induction machine (IM) is typically 2.5. Usually electric vehicles require CPSR values higher

*Corresponding Author Email: *Iarehpanahi@tafreshu.ac.ir* (M. Arehpanahi)

Please cite this article as: M. Arehpanahi, E. Kheiry, A New Optimization of Segmented Interior Permanent Magnet Synchronous Motor Based on Increasing Flux Weakening Range and Output Torque, International Journal of Engineering (IJE), IJE TRANSACTIONS C: Aspects Vol. 33, No. 6, (June 2020) 1122-1127

than 3 for over wide speed range. Therefore engineers try to increase the CPSR value by optimizing the design of electric machines which are specially based on induction machine and Permanent Magnet (PM) machine topologies. The CPSR of a permanent magnet motor could be improved by optimizing the rotor structure. One method of doing so is placing flux barriers in the rotor [4, 5]. Interior permanent magnet (IPM) synchronous motorsare often more widely considered for high CPSR and high efficiency applications such as electric vehicles and home appliances, because of their higher torque density in relation to other radial PM motors [6–8]. Many techniques for IPM flux-weakening improvement have been proposed in recent years [9–13]. Flux barriers design, PM segmented and various control strategies of IPM are the main focus of these literatures. In other words, these articles only improve the CPSR value while unwantedly decreasing the output torque in the final design. In this paper a new IPM optimization function for keeping the output torque at a nominal value and increasing the CPSR is proposed based on the combination of two variables i.e. normalized characteristic current and saliency ratio. The characteristic current is defined as d-axis flux divided by d-axis inductance. In this paper increasing the CPSR is carried out by decreasing the characteristic current, and output torque is adjusted by increasing the saliency ratio which leads to an increase in the reluctance torque component of IPM. In our new optimization function the CPSR value is controlled by characteristic current and output torque is adjusted by saliency ratio. Therefore these variables are optimized together using optimization of flux barrier shapes with PM segmented in rotor structure. For reducing calculations in the optimization process, a simplified magnetic equivalent circuit of SIPMSM is introduced. Using this equivalent circuit the d-q inductances and air gap flux values are obtained faster than 2D powerful numerical techniques such as Finite Element Method (FEM).

2. MAGNETIC EQUIVALENT CIRCUIT

Figure 1 shows the typical cross section view of SIPMSM. The magnetic flux line distribution of typical SIPMSM per pole is illustrated in Figure 1. A magnetic equivalent circuit of IPMSM has been presented in [12]. But in [12] the rotor PMs is not segmented. In this paper the PM segmentation effects is adopted to the [12] and the simplified SIPMSM is investigated. In SIPMSM there are two additional reluctances in comparison to the magnetic equivalent circuit of [12]. Therefore there are seven reluctances per pole in the proposed equivalent magnetic circuit of SIPMSM which is listed below:

Air gap, Iron bridge above the flux barrier, Leakage flux, Iron bridge between PMs, PM reluctance, Stator core andRotor core. Consequently, the modified equivalent magnetic circuit per pole considering PM segmentation is illustrated in Figure 2. Where $2\Re_g$, $\Re_{mm}$, $\Re_{ml}$, $\Re_{ib}$, $2\Re_{mosi}$, $\Re_r$, $\Re_s$ are reluctances of half of the air gap, iron bridges above the flux barrier, leakage flux, iron bridges between PMs, PM segmented, rotor and stator back iron respectively. φ_{rsi} and φ_g are ith PM segmented flux (i is the PM segmented number) and air gap flux respectively. There are three assumptions for rearrangement of Figure 2 which are each listed below:

The height and width of all PMs segmented and width of iron bridges between PMs is the same. This magnetic equivalent circuit of Figure 2 using above assumptions can be simplified to the proposed SIPMSM magnetic circuit which is illustrated in Figure 3.

In Figure 3, γ and $\Re_{mo}$ are the number of the PM segmented and PM segmented reluctances respectively. The relationship between flux pass through the iron bridges and between PMs λ_{ib} and λ can be expressed in Equation (1):

$$\begin{bmatrix}\lambda\\ \lambda_{ib}\end{bmatrix} \cong (1+2\eta+1/\beta)\begin{bmatrix}2\left(\frac{A_m}{A_{mm}}\right)\left(\frac{B_r}{B_{sbdg}}\right)-4 & -(\gamma-1)\\ -4 & \left(\frac{A_m}{A_{ib}}\right)\left(\frac{B_r}{B_{sib}}\right)-(\gamma-1)\end{bmatrix}\begin{bmatrix}\varphi_r\\ \varphi_{ib}\end{bmatrix} \quad (1)$$

where $\beta = \Re_g/\Re_{mo}$, $\eta = \Re_{mo}/\Re_{ml}$ and , A_m, A_{mm}, A_{ib} are cross section area of segmented PM, flux barrier and

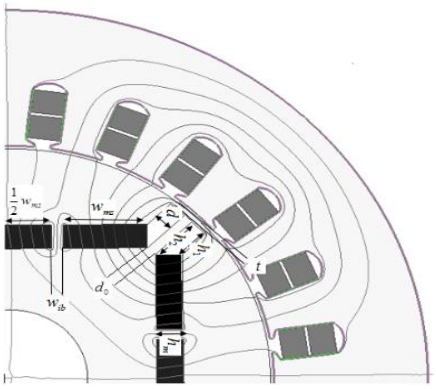

Figure 1. cross section view of SIPMSM per pole

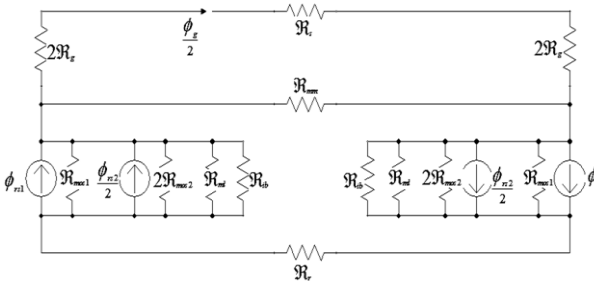

Figure 2. Magnetic equivalent circuit of SIPSM per pole

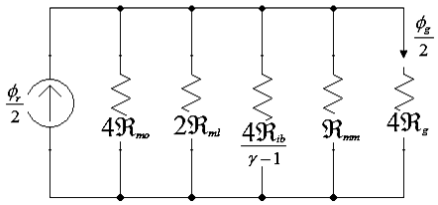

Figure 3. The simplified magnetic circuit of SIPMSM

iron bridge respectively. B_r, B_{sib}, B_{sbdg} are residual magnetic flux density of PM, saturation level of the magnetic flux density for iron bridges and flux barrier respectively. Saturation level of upper flux barrier and iron bridges is considered as 1.8T and 1.9T respectively.The d-q inductances of IPMSM are calculated by [13]. But for d-axis air gap the effect of PM segmentation i.e $(\gamma-1)\lambda_{ib}$ is added to [13] which is expressed in Equation (2):

$$g_d'' = \frac{k_c l_g}{k_{1ad} - k_1 k_{ad}/\left(1+\beta(1+2\eta+4\lambda+(\gamma-1)\lambda_{ib})\right)} \quad (2)$$

where L_l D, L $K_{w1}, N_{ph}, p, k_c$are leakage inductance, stator bore , machine axial length, winding coefficient, number of phase turns, pole pairs and carter coefficient. The coefficients k_{1ad}, k_{ad}, k_1 are expressed in the appendix. The specification of the motor and magnetic characteristic of the core (rotor and stator) which is called M-19 steel are illustrated in Table 1 and Figure 4. The design optimization in this paper for calculation of fluxes is carried out based on the simplified magnetic circuit of SIPMSM. Therefore verification of simplified magnetic circuit must be done. As a result the dq inductances and air gap flux of mentioned SIPMSM are evaluated by Finite Element Method (FEM) and simplified magnetic circuit.

The results of this comparison are listed in Table 2. Where w_{ms}, w_{ib}, h_m, d_0, d, , t h_2 are shown in Figure 1. It is seen that maximum error between simplified magnetic circuit and FEM is 3.5%, which is a very good result. Therefore to calculate inductance in the optimization process we used simplified magnetic circuit instead of FEM.

TABLE 1. Machine and PM parameters

Symbol	Value	Symbol	Value
l_g	0.5 mm	D	mm 82
N_{ph}	46	L	mm 55
γ	3	t	2 mm
d	mm 5.9	h2	4.2 mm
w_{ms}	mm 13	d_0	2.86 mm
w_{ib}	1.8 mm	h_m	mm 4
μ_{rec}	1.21	Br	(T) 1.1
Pole pairs	2	Hc	890kA/m
Nominal current	A 12	Nominal power	550 W
Nominal voltage	20.2 V	Nominal speed	1750 rpm

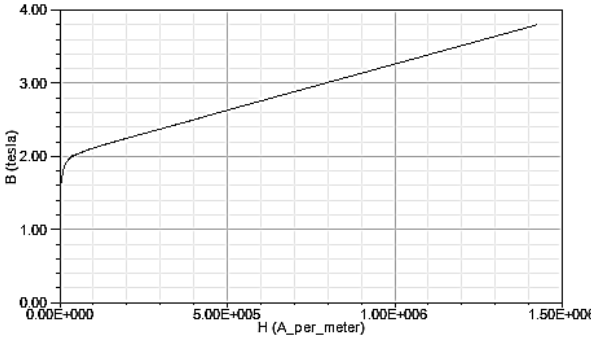

Figure 4. Magnetic characteristic of M-19 steel

TABLE 2. Simplified magnetic circuit and FEM results

Quantity	FEM	Modified magnetic circuit	Error (%)
d inductance(mH)	1.15	1.19	3.5
q inductance(mH)	3.12	3.09	0.96
PM linkage flux(mWb)	24.19	24.8	2.5

3. OPTIMIZATION OF SIPMSM FOR INCREASING CPSR AND OUTPUT TORQUE

Optimization of rotor structure is an interesting technique for increasing the CPSR value. In general the normalized characteristic current must be close to unity during the optimization process. The saliency ratio which depends on reluctance torque component of SIPMSM is added to the usual optimization function of SIPMSM for keeping the output torque at nominal value during CPSR improvement. The proposed optimization function for SIPMSM is expresses in Equation (3):

$$OF = min\left(k_1\left(\frac{\psi_{PMn}}{L_{dn}} - 1\right) + k_2\left(\frac{1}{\rho}\right)\right) \quad (3)$$

where L_{dn}, ψ_{PMn}, ρ are normalized values of the d inductance, PM flux and saliency ratio respectively. k_1, k_2 are pre-defined constant coefficients. Minimization of characteristic current and saliency ratio is highly dependent on d and q inductances values. These inductance values are dependent on PM and air bridges configuration in rotor structure too. Therefore a detailed design of rotor must be implemented. Figure 5 shows a detailed cross section view of SIPMSM rotor per pole.

In this paper six variables for optimization of (3) have been considered which are contained upper flux barrier bridge thickness "t" , distance between two neighbor flux barriers "$d_0 = DE$", flux barrier width "$d_1 = CD$", iron

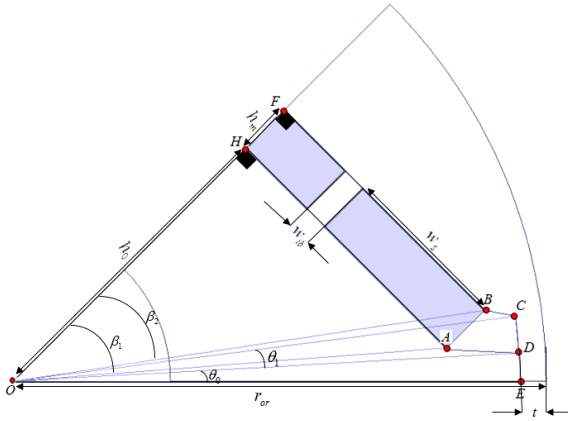

Figure 5. Cross section view of SIPMSM rotor per pole

bridge width between PM segmented "w_{ib}", distance between PM position and rotor centre"h_0" and number of PM segmented per poles "γ". Each segmented permanent magnet volume is considered constant which is equal to $3 \times 4 \times 13 = 156mm^3$. Then relation between thickness and length of segmented PM is calculated Equation (4):

$$w_s = \frac{156}{h_m \gamma} mm, \qquad HA = \frac{\gamma}{2} w_s + \frac{\gamma - 1}{2} w_{ib} = FB = w \tag{4}$$

where w_s, h_m are width and height of PM segmented respectively. According to Figure (5) the relationship between six design variables are expressed in Equations (5) - (12):

$$OE = r_{or} - t = r_b \tag{5}$$

$$sin(\angle DOE) = \frac{DE}{OE} = \frac{d_0}{r_b} \cong \theta_0, sin(\angle COD) = \frac{CD}{OD} = \frac{d_1}{r_b} \cong \theta_1 \tag{6}$$

$$\alpha = \frac{\pi/p - 2(\theta_0 + \theta_1)}{\pi/p} = 1 - \frac{2p(\theta_0 + \theta_1)}{\pi} \tag{7}$$

where p, α, r_{or} are poles pairs, pole pitch to pole arc ratio, and outer rotor radius respectively.

$$\angle HOA = \tan^{-1}\left(\frac{HA}{OH}\right) = \tan^{-1}\left(\frac{w}{h_0}\right) = \beta_1 \tag{8}$$

$$\angle FOB = \tan^{-1}\left(\frac{FB}{OF}\right) = \tan^{-1}\left(\frac{w}{h_0 + h_m}\right) = \beta_2 \tag{9}$$

$$OA = \sqrt{h_0^2 + w^2}, \qquad OB = \sqrt{(h_0 + h_m)^2 + w^2} \tag{10}$$

$$h_1 = BC = \sqrt{OB^2 + r_b^{\,2} - 2r_b OB \cos\left(\frac{\pi}{2p} - \beta_2 - \theta_0 - \theta_1\right)} \tag{11}$$

$$h_2 = AD = \sqrt{OA^2 + r_b^{\,2} - 2r_b OA \cos\left(\frac{\pi}{2p} - \beta_1 - \theta_0\right)} \tag{12}$$

As seen in Figure 5 increasing the "t" leads to an increase in the flux crossing through neighboring segmented PMs. As a result, the total air gap flux will be decreased, which will consequently reduce the output torque. If "t" has been selected to be very small the mechanical robustness of the rotor will decrease. An increase in the saliency ratio could possibly reduce the rotor's mechanical robustness due to the increasing "h_0", implying that the number of magnets segmented should be limited. Therefore optimization variables must be limited during optimization process. These limitations are as follows: $0.9 \le w_{ib}(mm) \le 3$, $0.8 \le t(mm) \le 3$, $19 \le h_0(mm) \le 29$, $2 \le \gamma \le 7$, $0.2 \le d_1(mm) \le 6$, and $1 \le d_0(mm) \le 3$.

The Genetic Algorithm (GA) technique is employed as an optimization tool. The SIPMSM is analyzed by FEM, then the OF is computed by FEM and simplified magnetic circuit results. The outputs of genetic algorithm and its typical design are listed in Table 3. It is shown that the number of segmented PM "γ"after optimization using GA is increased to 5 and flux barrier width d_1 has been decreased too. The magnet position "h_0" has been reduced due to increasing the number of PM segmented. The effect of these changes on inductances and rotor structure is illustrated in Figure 6 and Table 4. The output torque and other parameters are computed using commercial FEM Ansoft/Maxwell software. The optimized SIPMSM has higher torque, current angle and saliency ratio related to the typical design. Increasing the saliency ratio increases the reluctance torque component, increasing the output torque and power as a result. Increasing the d inductance in optimized design leads to a decrease in the air gap flux, decreasing the magnetic torque component. But the increase in the reluctance torque component is greater than the decrease in the magnetic torque component. As a result the total output torque increases by 11% compared to the typical design. The output torque of typical and optimized SIPMSM is illustrated in Figure 7. According to Figure 7,maximum speed of the optimized design in generation of output torque is higher than typical design. The characteristic current of optimized SIPMSM is decreased by 30% compared to the typical design, leading to an increase in

TABLE 3. Design variables before and after optimization

Parameter	Before optimization	After optimization
γ	3	5
$w_{ib}(mm)$	1.8	1.07
$t(mm)$	2	1.63
$h_0(mm)$	27.82	22.98
$d_0(mm)$	2.86	2.06
$d_1(mm)$	5.94	1.4

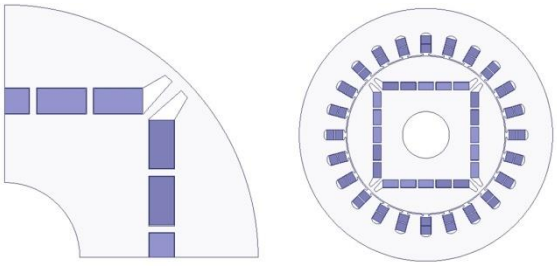

Figure 6. The cross section view of optimized SIPMSM

TABLE 4. typical and optimized machine parameter

Parameter	Before optimization	After optimization
ψ_{PM} (mWb)	24.19	21.05
L_d (mH)	1.064	1.3
L_q (mH)	3.12	4.18
ψ_{PMn}/L_{dn}	1.89	1.35
ρ	2.93	3.22
T (N.m)	1.845	2.05

CPSR. Figure 8 shows a comparison of the output power versus rotor speed which is obtained by typical and optimized design. Based on Figure 8 it is clear that the optimized design flux weakening range is higher than typical design. In other words, the CPSR of optimized design is increased from $\frac{5700}{1750} = 3.25$ to $\frac{10900}{1750} = 6.22$, which is a noticable improvement.

The voltage limitation of SIPMSM using dynamic voltage equation is expressed in Equation (13):

$$V_d^2 + V_q^2 = (\omega L_q)^2 I_q^2 + (\omega L_d)^2 \left(I_d + \frac{\psi_{PM}}{L_d}\right)^2 \leq V_{smax}^2 \quad (13)$$

where V_{smax} is the maximum value of stator voltage. The Equation (19) demonstrates that the trajectory of stator current components in dq coordinate is an elliptical curve with centre (0 ,- $\frac{\psi_{PM}}{L_d}$).

Figure 9 showe stator current trajectory of both typical and optimized designs. In optimized design (Figure 9-b) the centre of voltage limitation locus is closer to the centre of current limitation locus compared to the typical design,therefore the maximum accessible speed of optimized design increases compared to typical designs. Comparison of torque components which are obtained by typical and an optimized design is illustrated in Figure 10. This demonstrates that the electromagnetic torque component of optimized SIPMSM (Figure 10-a) in all current angle ranges is smaller than the typical design but the reluctance torque component of optimized design is higher than typical design in all ranges of the current angle (Figure 10-b). Finally, by addition of two torque components of optimized design which is equal to total output torque is higher than total output torque of typical design (Figure 10-c) excluding current angles lower than 15 degrees which are belong to light loads. This range is not important because nominal current angle operation of SIPMSM is at least out of this range.

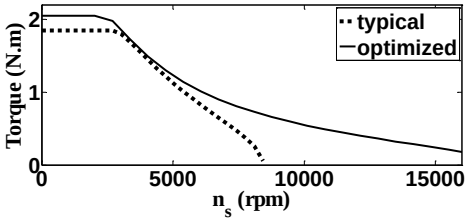

Figure 7. Torque-speed of typical/optimized SIPMSM

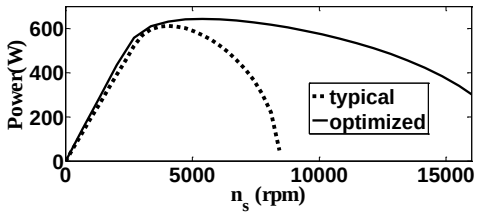

Figure 8. Power-speed typical/optimized SIPMSM

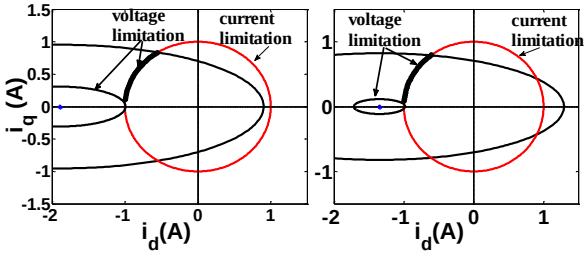

Figure 9. Current trajectory of SIPMSM a-typical, b-optimized

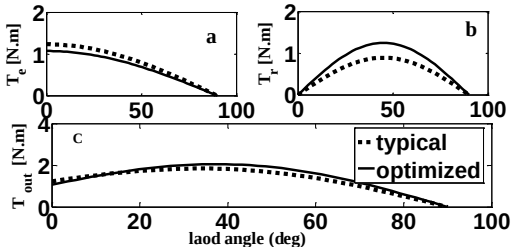

Figure 10. Torque component and output torque of typical and optimized SIPMSM versus stator current angle

4. CONCLUSION

In this paper, an optimal design of a segmented interior permanent magnet synchronous motor (SIPMSM) for increasing the flux weakening range based on minimization of characteristic current and saliency ratio

is proposed. The new objective function is well defined using a combination of characteristic current minimization (for increasing the flux weakening range) and maximization of saliency ratio (for compensation of output torque drop during optimization process). In order to reduce calculations , magnet flux and dq inductances are calculated a using the proposed simplified magnetic equivalent circuit instead of FEM analysis. Simulation results demonstrate that the optimized design has a good performance in increasing the flux weakening range and output torque related to the typical design.

5. REFERENCES

1. Moradi CheshmehBeigi, H., "Design and simulation of a moving-magnet-type linear synchronous motor for electromagnetic launch system", ***International Journal of Engineering - Transaction C: Aspects***, Vol. 30, No. 3, (2017), 351–356.
2. Sahebjam, M., Bannae Sharifian, M.B., Feyzi, M.R. and Sabahi, M., "Novel Unified Control Method of Induction and Permanent Magnet Synchronous Motors", ***International Journal of Engineering - Transaction B: Applications***, Vol. 32, No. 2, (2019), 256–269.
3. Aghazadeh, H., Afjei, E. and Siadatan, A., "Comprehensive Design Procedure and Manufacturing of Permanent Magnet Assisted Synchronous Reluctance Motor", ***International Journal of Engineering - Transaction C: Aspects***, Vol. 32, No. 9, (2019), 1299–1305.
4. Seo, J.H. and Choi, H. S., "Analytical modeling for calculating cogging torque in interior permanent magnet machine with multi flux-barriers", ***IEEE Transactions on Applied Superconductivity***, Vol. 24, No. 3, (2014), 1–4.
5. Parasiliti, F., Villani, M., Lucidi, S. and Rinaldi, F., "Finite-element-based multiobjective design optimization procedure of interior permanent magnet synchronous motors for wide constant-power region operation", ***IEEE Transactions on Industrial Electronics***, Vol. 59, No. 6, (2011), 2503–2514.
6. Pouramin, A., Dutta, R. and Rahman, M. F., "Design Optimization of a Spoke-Type FSCW IPM Machine to Achieve Low Torque Ripple and High Torque Density under a Wide Constant Power Speed Range", In 2018 Ieee Energy Conversion Congress and Exposition (Ecce), IEEE, (2018), 6914–6921.
7. Arehpanahi, M. and Sanaei Torab, V., "Optimal design of interior permanent magnet motor with wide flux weakening range", ***Scientia Iranica***, Vol. 22, No. 3, (2015), 1045–1051.
8. Pietrini, G., Soldati, A., Concari, C. and Bianchi, N., "General Magnetic Model for the Analysis and Optimization of Multiple Barrier Rotors", In 2018 IEEE Energy Conversion Congress and Exposition (ECCE), IEEE, (2018), 6937–6944.
9. Bolognani, S., Calligaro, S. and Petrella, R., "Adaptive flux-weakening controller for interior permanent magnet synchronous motor drives", ***IEEE Journal of Emerging and Selected Topics in Power Electronics***, Vol. 2, No. 2, (2014), 236–248.
10. Bolognani, S., Calligaro, S., Petrella, R. and Pogni, F., "Flux-weakening in IPM motor drives: Comparison of state-of-art algorithms and a novel proposal for controller design", In Proceedings of the 2011 14th European Conference on Power Electronics and Applications, IEEE, (2011), 1–11.
11. Hoang, K.D., Wang, J., Cyriacks, M., Melkonyan, A. and Kriegel, K., "Feed-forward torque control of interior permanent magnet brushless AC drive for traction applications", In 2013 International Electric Machines & Drives Conference, IEEE, (2013), 152–159.
12. Alsawalhi, J.Y. and Sudhoff, S. D., "Effects of positioning of permanent magnet axis relative to reluctance axis in permanent magnet synchronous machines", In 2015 IEEE Power and Energy Conference at Illinois (PECI), IEEE, (2015), 1–8.
13. Hwang, C.C., Chang, S.M., Pan, C.T. and Chang, T. Y., "Estimation of parameters of interior permanent magnet synchronous motors", ***Journal of magnetism and magnetic materials***, Vol. 239, No. 1–3, (2002), 600–603.

6. APPENDIX

$$k_{1ad} = \alpha + \frac{sin(\alpha\pi)}{\alpha} \quad \text{(A1)}$$

$$k_{\alpha d} = \frac{sin(\alpha\pi/2)}{\alpha\pi/2} \quad \text{(A2)}$$

$$k_1 = 4\,sin(\alpha\pi/2)/\pi \quad \text{(A3)}$$

$$\Re_{ml} = \frac{2d}{\mu_0 A_{ml}} = \frac{4d}{\mu_0 L(h_1+h_2)} \quad \text{(A4)}$$

$$\Re_{mm} = \frac{2d+d_0}{\mu_0 \mu_{re} A_{mm}} = \frac{2d+d_0}{\mu_0 \mu_{re} Lt} \quad \text{(A5)}$$

$$\Re_{ib} = \frac{h_{ib}}{\mu_0 \mu_{re} A_{ib}} = \frac{h_{ib}}{\mu_0 \mu_{re} L w_{ib}} \quad \text{(A6)}$$

$$\varphi_{rsi} = B_r L w_{msi} = B_r L \frac{w_m}{3} = \frac{\varphi_r}{3} \quad \text{(A7)}$$

Persian Abstract

چکیده

در این مقاله یک تابع بهینه‌سازی جدید برای افزایش ناحیه تضعیف شار و گشتاور خروجی موتور مغناطیس دائم تکه تکه شده ارائه شده است. در روش پیشنهادی از دو پارامتر نسبت برجستگی و جریان مشخصه بطور همزمان در تابع هدف استفاده شده است. تمرکز این مقاله بر روی تغییر ساختار روتور است با در نظر گرفتن طراحی موانع شار در روتور. طراحی دقیق با جزییات روتور با استفاده از مدار معادل ساده شده پیشنهادی آورده شده است. خروجی مدار معادل پیشنهادی از نظر محاسبه اندوکتانس‌های دو محوری و شار پیوندی با نتایج اجزاء محدود تایید شده‌اند. نتایج شبیه‌سازی نشان می‌دهد که موتور بهینه‌شده دارای دو برابر ناحیه تضعیف شار بزرگتر نسبت به طراحی معمولی است.